This paper is part of the Proceedings of the 14th International Conference on Simulation and Experiments in Heat Transfer and its Applications (HT 2016)
www.witconferences.com

Effect of processor layout on the thermal performance of fully immersed liquid-cooled microelectronics

Y. Al-Anii[1,2], A. Almaneea[1], N. Kapur[1],
J. Summers[1] & H. Thompson[1]
[1]*Institute of ThermoFluids, University of Leeds, UK*
[2]*University of Anbar, Iraq*

Abstract

The natural convection cooling system of a fully immersed server in a dielectric liquid is analysed numerically, where the servers are in sealed capsules and submerged in a dielectric fluid. A reduced order flow model is developed under a saturated porous media flow assumption using a Darcy flow regime and the Stokes equations solved numerically using successive over relaxation and time marching techniques. The simplified model is shown to agree well with predictions from full Navier–Stokes flow analyses and then used to study the role of spatial parameters on the convective heat transfer, in particular the effect of the locations and separations of two heat sources representing two central processing units (CPUs). The flow and heat transfer characteristics are analysed for a range of modified Rayleigh numbers between 0.5 and 300 and a correlation for Nusselt number is obtained which shows that the thermal behaviour is most strongly influenced by the modified Rayleigh number and that the vertical separation of the CPUs is more influential than the vertical position of the lower CPU.
Keywords: convective cooling of server, Darcy flow, liquid-immersed server, porous media.

1 Introduction

The increasing demand for digital services such as telecommunication, social media, financial services and information systems are supported by large warehouses of servers, called data centres, where digital information is processed,

stored and communicated. The increase in power consumed by data centres leads to more heat being generated, which in turn requires more than 30% of the data centre energy budget to remove it [1, 2]. Cooling of, or harvesting, the heat from a data centre can be achieved by either air or liquid. Most traditional data centres currently use air, however liquid is more effective as they can typically carry 1000 times more thermal energy per unit volume than air and can therefore handle high density data centres [3]. There are naturally three techniques of heat removal using liquids, each in progressively greater proximity to the electronics: rear door rack heat exchangers [4], on server or on chip heat exchangers [5] and liquid immersion [6, 7]. In the latter case, the fluid used is a dielectric liquid that is in direct contact with all of the microelectronics encapsulated vertically on one of the capsule's walls and the heat is transferred to the opposite, cooler wall via a natural convection current. In this study, the geometrical investigation of an immersed server is carried out by assuming the fluid flow in the capsule, which is the container of server and cooling technology, is governed by creeping flow in a saturated porous media in the presence of buoyancy forces. The use of such a reduced order model enables a wide-ranging parameter study to be carried out in feasible timescales.

Similar to the enclosed server capsule discussed earlier, Nithiarasu *et al*. [8] studied a square cavity filled with fluid in a saturated porous media where the left wall is hot and the right wall is cold while the top and bottom walls are insulated. The study demonstrated that both Rayleigh number and porosity affects the wall Nusselt number. Chan *et al.* [9] numerically studied a rectangular cavity enclosure with fluid and porous media. The top and bottom walls are insulated and the heat is transferred from the left wall and the enclosure is cooled by constant temperature on the right wall. The paper showed that the convective motion and temperature field distortion both increase with Rayleigh number. The paper also presented a correlation that was obtained from three parameters, i.e. the Rayleigh number, Darcy number, and the cavity's geometric aspect ratio. Poulikakos and Bejan [10] also investigated an enclosure with a fluid saturated porous media with hot and cold sources on each side of the enclosure. A part of the left wall was hot and the other part was cold while the remaining walls were insulated. The investigation found that in the situation when the hot part was above the cold part the natural circulation was either incomplete vertical penetration or incomplete horizontal penetration. However, as expected, in the case when the cold part was above the hot part the flow spreads throughout the porous medium. Ismaeel [11] carried out an enclosure model with a hot patch on one side and a cold patch on the other side. The study demonstrated that the best heat transfer performance was obtained when the hot patch was at the bottom and the cold patch at the top. In contrast, the lowest heat transfer performance occurred when the hot patch was placed at the top and the cold patch at the bottom. Other investigations analysed the situation when the heat was from below for enclosures that had fluid saturated porous media with different parameters [12, 13]. Kladias and Prasad [14] studied the effect of the Prandtl and Darcy numbers for fluid flow in a porous media where the heat was generated from the bottom of the enclosure and the study showed that the

convective heat transfer regime increased with increasing Rayleigh number, Darcy number and Prandtl number.

This paper studies natural convection in an enclosed vertically aligned server capsule with two heat sources, representing lower and upper central processing units (CPUs) (Figure 1(a)). The server is immersed in a porous medium with a saturated (dielectric) fluid. Heat is transferred from the two heat sources to the working fluid, which is then removed by the cold wall on the opposite side of the capsule. Results show that the position of the heat source has a strong influence on the heat transfer process.

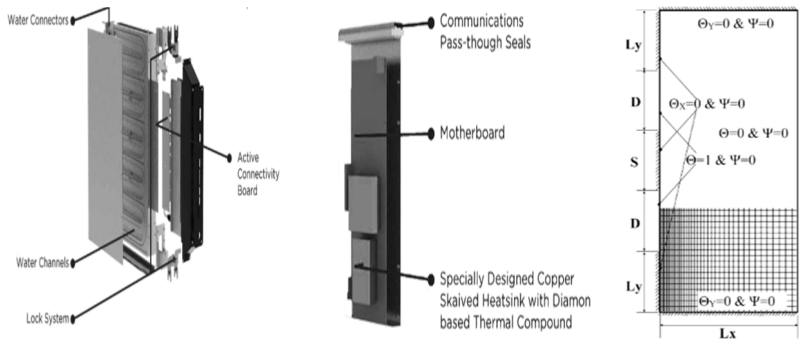

Figure 1: (a) Server design, and (b) numerical model, mesh and boundary conditions.

2 Model description

The present study deals with immersion of a dual CPU server inside a vertically aligned capsule. The capsule is filled with dielectric liquid, which removes heat from the CPUs by a naturally driven convective circulation. Convective circulation can move freely inside the capsule from the heat source on one vertical wall of the capsule to the opposite vertical wall, which is acting as a heat sink. However, fluid flow is impeded by the presence of the many microelectronic features of the server. For example, a basic server contains heat sinks (fins or spreaders), banks of random access memory (RAM), power supply and additional on board components such as network or service processors. All of these components impede the coolant flow and can inhibit the natural convection inside the encapsulated server, which in turn reduces the heat transfer capability.

The two dominant forces acting on the fluid flow are in competition, namely coolant buoyancy forces of the natural convection and the viscous forces due to the microelectronic components and capsule walls. Flow is therefore modelled by natural convection inside a saturated porous medium. The liquid inside the porous medium represents the coolant, whereas the microelectronic components represent the solid structure of the porous medium.

3 Mathematical model

The flow model employs a number of simplifying assumptions. Here, the flow in the server capsule is modelled as an isotropic porous layer with the additional assumptions of: (i) single-phase flow; (ii) thermodynamic equilibrium between the porous components and the saturated fluid; (iii) Boussinesq's buoyancy approximation is valid; (iv) flow is slow so that fluid inertia can be neglected; (v) flow in the porous media is based on Darcy's law; (vi) chemical reactions and viscous heating are neglected.

The governing equations based on the conservation of mass, momentum and energy are listed respectively using vector notation [15] as:

$$\nabla \cdot \vec{v} = 0 \tag{1}$$

$$\vec{\mathrm{v}} = -(\mathrm{K}/\mu)[\nabla \mathrm{p} - \rho \vec{\mathrm{g}}] \tag{2}$$

$$\sigma(\partial \mathrm{T}/\partial \mathrm{t}) + \vec{\mathrm{v}} \cdot \nabla \mathrm{T} = \alpha \nabla^2 \mathrm{T} \tag{3}$$

The density in the body force term of equation (2) varies according to the Boussinesq's approximation that density varies with temperature. Mathematically, the Boussinesq's approximation is written as

$$\rho = \rho_\infty [1 - \beta(T - T_\infty)] \tag{4}$$

where β is the fluid volumetric thermal expansion coefficient and ρ_∞ is the liquid density at the balance temperature T_∞. Equations (1–3) with appropriate boundary conditions can provide both the local velocity components and temperature. The problem can, in fact, be simplified to two dependent variables by representing each velocity component in terms of the stream-function, which in addition to making the numerical problem simpler, facilitates flow visualisation. Physically, both horizontal and vertical components of velocity can be represented by stream-function derivatives as shown in equations (5) and (6).

$$u = \frac{\partial \psi}{\partial y} \tag{5}$$

$$v = -\frac{\partial \psi}{\partial x} \tag{6}$$

The reduction of the momentum equation (2) to a single component equation is achieved by taking the cross product of equation (2), resulting in equation (7) as follows

$$\nabla \times \vec{v} = \left(\frac{\partial v}{\partial x} - \frac{\partial u}{\partial y}\right)\vec{k} = \frac{K}{\mu}(\nabla \times \nabla p) + \left(\frac{Kg}{\mu}\frac{\partial \rho}{\partial x}\right)\vec{k} \tag{7}$$

The stream-function formulation automatically conserves mass and therefore the final form of the momentum and energy equations is as follows,

$$\nabla^2 \psi = -(Kg\rho\beta/\mu)\, T_x \tag{8}$$

$$\alpha \nabla^2 T = T_t + \left(T_x \psi_y - T_y \psi_x\right) \tag{9}$$

4 Numerical solution

The solution procedure of equations (8) and (9) requires four steps, which are explained in detail in this section. The first step non-dimensionalises equations (8) and (9) to introduce the important non-dimensional parameters.

4.1 Dimensionless formulation

In order to non-dimensionalise equations (8) and (9), all independent (x, y, t) and dependent (ψ, T) variables need to be defined in terms of characteristic values, this is achieved by the following non-dimensional procedure [16].

$$X = \frac{x}{D}\ ,\ Y = \frac{y}{D}\ ,\ \Psi = \frac{\psi}{\alpha}\ ,\ \tau = \frac{t\alpha}{D^2}\ \ and\ \ \theta = \frac{(T-T_\infty)}{(T_S-T_\infty)} \tag{10}$$

Substituting equations (10) into equations (8) and (9), and then grouping dimensional terms to obtain the non-dimensional characteristics numbers called Rayleigh number, Ra, and Darcy number, Da, as in equation (11):

$$Ra = \frac{g\beta\rho D^3\Delta T}{\alpha\mu}\ ,\ Da = \frac{K}{D^2} \tag{11}$$

These two non-dimensional numbers can be combined to define a modified Rayleigh number, $Ra^* = Ra\ Da$.

Re-arranging the non-dimensional governing equations yields equations to be used in subsequent steps.

$$\nabla^2\Psi = -Ra^*\,\theta_X \tag{12}$$

$$\theta_\tau = \nabla^2\theta - (\theta_X\Psi_Y - \theta_Y\Psi_X) \tag{13}$$

4.2 Solution procedure

Firstly, the resulting equations (12) and (13) should be transformed from partial differential equation (PDE) forms to linear algebraic forms using the finite differences method FDM. The discrete equations contain spatial and time dependent terms, rather than first and second order discretisation terms. The final form of the momentum equation (12) results as an elliptic, Poisson type equation, which is solved using successive over relaxation, SOR. In brief, this method solves for the entire nodal point with respect to the values of neighbourhood nodal points. For each nodal point, iterations repeat for a specific time until convergence, where the error $< 10^{-4}$ enables the desired final values of entire distribution of stream function to be obtained.

On the other hand, the energy equation (13) is parabolic with time dependency. A time marching technique is employed as the optimal method of solution, where the growth of the function distribution is based on a convergence error of the order of 10^{-6}. Since a steady state solution will emerge, the dependency of the energy equation upon time will vanish after a period of successive time intervals and convergence is reached. The reduced and formulated finite difference forms of the two governing equations are written as follows:

$$\Psi_{i,j}= f_1\left(\Psi_{i-1,j}, \Psi_{i,j+1},\Psi_{i,j-1},\Psi_{i+1,j}\right)+(Ra^*)f_2\left(\theta_{i,j}, \theta_{i+1,j}\right) \quad (14)$$

$$\theta_{i,j}^{\tau+1}=f_3\left(\theta_{i-1,j}^{\tau},\theta_{i,j}^{\tau},\theta_{i,j+1}^{\tau},\theta_{i,j-1}^{\tau},\theta_{i+1,j}^{\tau}\right)-\left[f_4\left(\theta_{i-1,j}^{\tau},\Psi_{i,j+1}^{\tau},\Psi_{i,j-1}^{\tau},\theta_{i+1,j}^{\tau}\right) - f_5\left(\Psi_{i-1,j}^{\tau},\theta_{i,j+1}^{\tau},\theta_{i,j-1}^{\tau},\Psi_{i+1,j}^{\tau}\right)\right] \quad (15)$$

4.3 Parametric criteria, mesh and boundary conditions

The geometry of the current case study is represented by a two-dimensional rectangular cell. It is of fixed width Lx=1U and variable height Ly. In addition, the distance between the two heat sources, S, is varied. The studied non-dimensional range is S=0.5, 0.75, 1.0, 1.25, 1.5, 2.0, 2.5 and 3.0 each with respect to the 1U width. For each of the Ly values 1, 1.5, 2 and 3, the modified Rayleigh number is also varied independently in the range Ra*=0.5, 1, 5, 10, 20, 50, 100, 200 and 300.

The mesh of the domain is graduated toward the CPUs in order to investigate the thermal behaviour more accurately. For the mesh stretching process, the x-axis nodal points are re-distributed by defining a slope of distribution of 0.2, and damping factor of 2 [17]. Equations (16) and (17) give the criteria of these values and the new position of the nodal point.

$$x = x_{i=1} - \Gamma(x_{i=1} - x_{i=imax}) \quad (16)$$

where, Γ depends on a non-dimensional position value Λ given by the expression below

$$\Gamma = 0.2\,\Lambda + 0.8\left(1 - \frac{tanh(2-2\Lambda)}{tanh(2)}\right) \quad (17)$$

Liquid in the capsule is heated by two heat sources, namely the lower and upper CPUs. In the meantime, upper and lower edges of the capsule are insulated, which ensures that all the heat captured by the fluid is transported to the opposite side, where the heat is collected in the primary water circuit, which is modelled by a constant zero non-dimensional temperature condition. In addition, the left edges of the capsule below the lower CPU (of length Ly) and between the CPUs (of length S) are insulated. The geometrical dimensions, nodal mesh and boundary conditions are illustrated above in Figure 1(b).

4.4 Code validation

The flow model is first compared with the study of Bejan and Kraus [15], who analysed natural convection in a vertical layer porous media and it can be seen in Figure 2 shows very good agreement with their predictions of the average Nusselt number versus modified Rayleigh number.

The current simple model is now compared with the corresponding predictions from solutions of the full two-dimensional Navier–Stokes for natural convection using COMSOL. With the same geometry and boundary conditions and a Rayleigh number of 50,000 the solutions of the two models are compared. For the simplified model the modified Rayleigh number, Ra*, and Darcy number are set to 50 and

10^{-3} respectively. The Nusselt number is calculated in both cases for a range of CPU configurations and is presented in Figure 3. The average error between results for all cases is less than 5%, and suggests that the porous medium modelling assumptions are valid.

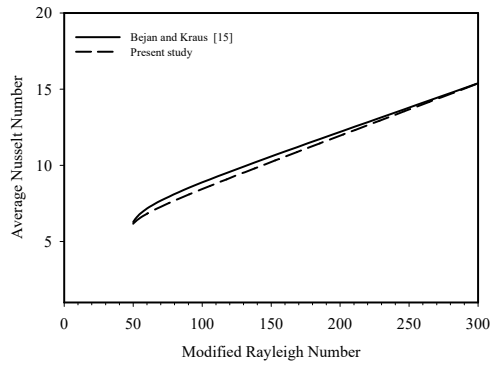

Figure 2: Average Nusselt number vs. modified Rayleigh number for present study and Bejan and Kraus [15].

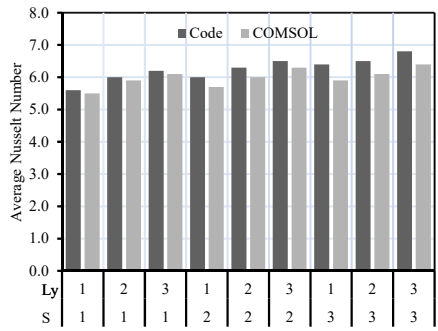

Figure 3: Average Nusselt number comparison between the simplified model (based on the FDM code) and full Navier–Stokes (using COMSOL) with Ra=50,000.

5 Results and discussion

In this study, the liquid in the capsule is heated by two CPUs. These CPUs supply heat to the capsule from one side and as a result, the generated heat creates convection currents, which are responsible for carrying the heat plume away from the heat-sources to where the heat can be rejected into the water loop passing through the opposite side of the capsule. The positions of the CPUs are represented using two spatial parameters, namely Ly, the vertical distance of the first CPU from the bottom of the capsule, and S, the vertical spacing between the CPUs. The

heating fluxes, which are related to the workload of the CPUs, are represented by varying the Rayleigh number.

Figure 4(a) presents the ratio of the fluid velocity at grid points adjacent to the lower CPU to corresponding velocities along the CPUs in order to show interactions between the thermal plumes associated with each CPU. Ly has an influence on the patterns of velocity ratio and as Ly increases the velocity ratio slightly decreases. For example, for Ly=1U, the velocity at the leading edge of lower CPU is smaller than the similar position of the upper one. It can be seen that the heating effect of the lower CPU is initially more abrupt than at the upper one since in the latter case the cooling fluid is already carrying more thermal energy. However, as the liquid moves up the upper CPU the velocity increases more quickly due the thicker thermal boundary layer and this effect is particularly strong for the upper quarter of the upper CPU. Furthermore, when Ly is set to 3U, the mean velocity above the upper CPU is significantly bigger than over the upper CPU due to the larger distance to the upper edge of the capsule. Figure 4(a) suggests that Ly=1.5 represents a critical value since the trend of decreasing velocity above the CPUs (for Ly<1.5) changes to that of increasing velocity above the CPU for Ly>1.5.

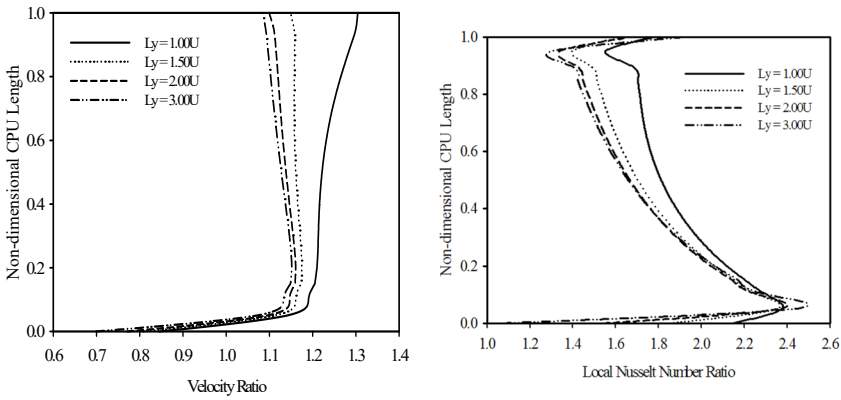

Figure 4: Effect of non-dimensional position of CPUs on ratios of (a) non-dimensional velocity and (b) local Nusselt number, at S=1 and Ra*=50.

From a heat transfer perspective, the boundary layer thickness has a direct effect on the heat removal from the CPUs. This is investigated via the local Nusselt number being calculated along unit each CPU. As with the velocity ratios shown in Figure 4(a), the ratio of local Nusselt numbers for the lower to upper CPUs is plotted in Figure 4(b). For Ly=1, the lower CPU has a local Nusselt number that is on average twice that of the upper CPU. The upper CPU has a thicker boundary layer since the fluid adjacent to it is hotter because it is located closer to the lower CPU, i.e. S=1U. Therefore, the ability of the dielectric fluid to remove heat from

the upper CPU is reduced. As Ly increases the ratio of the two local Nusselt numbers decreases, since the boundary layer thicknesses over both CPUs are similar. It can also be see that the influence of Ly on the local Nusselt number ratio reduces since Figures 4(a) and (b) show marginal differences between Ly=2 and Ly=3.

The effect of the vertical CPU separation, S, is now investigated and the results are shown in Figure 5. As S increases, the velocity ratio decreases incrementally as can be seen in Figure 5(a) and the opportunity to re-accelerate the convection current is increased, resulting in a decrease of the velocity ratio.

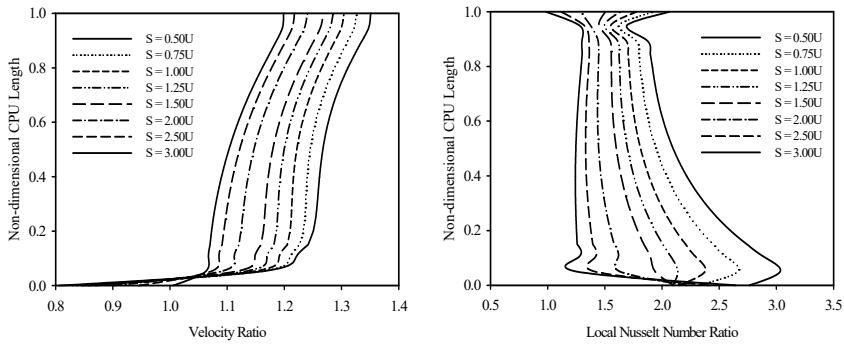

Figure 5: Effect of non-dimensional position of CPUs on ratios of (a) non-dimensional velocity and (b) local Nusselt number, at Ly=1 and Ra*=50.

The effect of increasing S on the Nusselt number is more interesting, as shown in Figure 5(b). When S is small, there is a strong interaction between the convection currents over the CPUs and the lower current influences the upper one over the first quarter of upper CPU's length, leading to a lower local Nusselt number that is three times greater than the upper one. As S increases the Nusselt number over the lower CPU is still higher than that over the upper CPU, however the latter is increasing towards the former. For S values greater than 2U, the Nusselt number over the lower CPU is approximately constant while over the upper CPU it increases. This occurs since the greater vertical separation of the CPUs enables the dielectric liquid to cool before it reaches the upper CPU, which results in a greater acceleration of the convection current over the upper CPU.

The streamlines and isotherms are related since the fluid circulation is a function of density change, which is also dependent on the local temperature gradient. Figure 6 shows stream-lines for different values of the modified Rayleigh number and as the buoyancy forces are increased with increasing modified Rayleigh number, the stream-lines are displaced upwards and the convection current strengthens due to the larger local temperature differences shown in Figure 6. It is clear that as the modified Rayleigh number increases the maximum

stream function value increases (implying a faster natural convection current) resulting in a larger average Nusselt number.

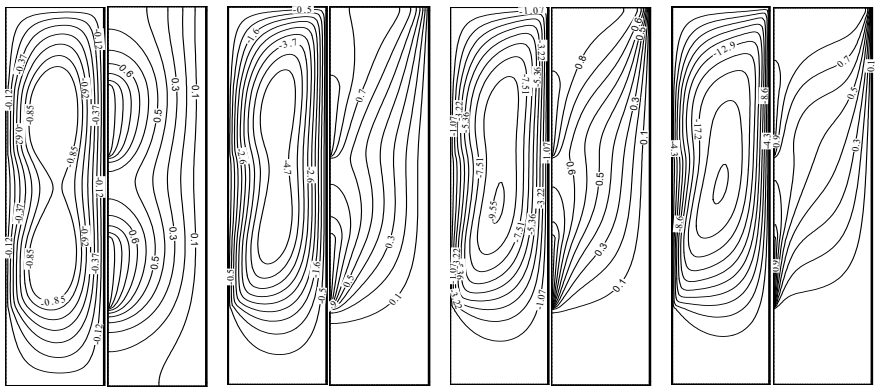

(a) (b) (c) (d)

Figure 6: Streamlines (left) and isotherms (right) for Ly=S=1U at (a) Ra*=10, (b) Ra*=50, (c) Ra*=100 and (d) Ra*=300.

This increased heat transfer is shown more clearly by the relationship between average Nusselt number and modified Rayleigh number, presented in Figure 7. The data can be described by a single correlation equation, which highlights the influence Ra*, Ly and S on the average Nusselt number. A Gauss-Newton technique is employed in obtaining this correlation and the result is shown in equation (18). The correlation coefficient between the curve (18) and the computational data is 0.968.

$$Nu = 0.801\, Ra^{*0.5} Ly^{0.075} S^{0.085} \tag{18}$$

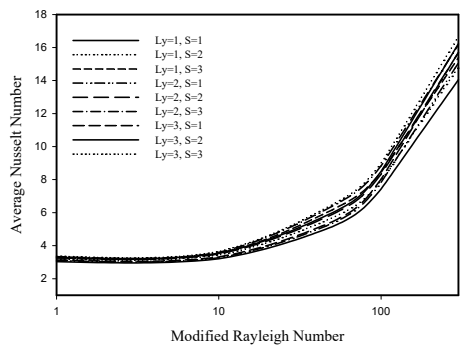

Figure 7: Average Nusselt number vs. modified Rayleigh number for all spatial ratios.

6 Conclusion

The natural convective cooling of servers in sealed enclosures provides an alternative means of cooling high density microelectronics. The much higher heat capacity of dielectric liquids compared to, for example, traditional air cooling methods by obviating the need to pump or blow the coolant. Since the flow paths of the convection currents affect the heat transfer process, this study has illustrated, using a simplified model, the effect of both buoyancy and geometric parameters on this process.

Since most servers contain two or more CPUs the heat transfer is dependent on the spatial layout of the CPUs. Summarising the computational results in the form of an empirical correlation shows that the heat transfer, expressed as average Nusselt number, is strongly influenced by the modified Rayleigh number, Ra*, and that the vertical separation, S, of the CPUs is more influential than the vertical position of the lower CPU, Ly.

Nomenclature

D	Length of the CPU = 1U	Ly	Edge to CPU space	U	Server unit length= 1.75 inches
f	Finite difference function	p	Dimensional pressure	u, v	Velocity vectors
g	Gravitational acceleration	S	CPUs In-between space	x, y	Dimensional coordinate
K	Permeability	t	Time	X, Y	Dimensionless coordinate
Lx	Width of capsule = 1U	T	Temperature		
Greek symbols					
α	Thermal diffusivity	Λ	Place value	τ	Dimensionless time
β	thermal expansion factor	μ	Viscosity	ψ	Dimensional stream-function
Γ	Stretching function	ρ	Density	Ψ	Dimensionless stream-function
θ	Dimensionless temp	σ	Heat capacity ratio		
Subscripts and superscripts					
1-5	Finite difference notation	t	Time derivative	$\tau+1$	Next time step
i, j	Nodal coordinate	x, y	Spatial derivative	∞	Infinite medium
s	Surface	τ	Current time step		

Acknowledgements

The authors thank the Higher Committee for Education Development (HCED) in Iraq and Saudi Cultural Bureau for their sponsorships. The authors would also like to thank Iceotope Ltd for providing inspiration for the application.

References

[1] Shah, A., *et al*. Impact of rack-level compaction on the data center cooling ensemble. in Thermal and Thermomechanical Phenomena in Electronic Systems, 2008. ITHERM 2008. 11th Intersociety Conference, 2008, IEEE.

[2] Greenberg, S., *et al*. Best practices for data centers: Lessons learned from benchmarking 22 data centers. Proceedings of the ACEEE Summer Study on Energy Efficiency in Buildings in Asilomar, CA. ACEEE, August 2006, **3**, 76-87.
[3] Pacific Gas and Electrical. High Performance Data Centers, 2011.
[4] Almoli, A., *et al*. Computational fluid dynamic investigation of liquid rack cooling in data centres. Applied Energy, 2011.
[5] Chien-Yuh, Y., *et al*. An in-situ performance test of liquid cooling for a server computer system. in 2010 5th International Microsystems, Packaging, Assembly and Circuits Technology Conference (IMPACT 2010), 20–22 October 2010. Piscataway, NJ, USA: IEEE.
[6] Chester, D., *et al.* Cooled electronic system, Patents US20130208421 A1, 2013.
[7] Hopton, P. and J. Summers. Enclosed liquid natural convection as a means of transferring heat from microelectronics to cold plates. in Semiconductor Thermal Measurement and Management Symposium (SEMI-THERM), 29th Annual IEEE, 2013. IEEE.
[8] Nithiarasu, P., K. Seetharamu, and T. Sundararajan. Natural convective heat transfer in a fluid saturated variable porosity medium. International Journal of Heat and Mass Transfer, 1997, **40(16)**, 3955-3967.
[9] Chan, B., C. Ivey, and J. Barry. Natural convection in enclosed porous media with rectangular boundaries. Journal of Heat Transfer, 1970. **92(1)**, 21-27.
[10] Poulikakos, D. and A. Bejan. Natural convection in a porous layer heated and cooled along one vertical side. International Journal of Heat and Mass Transfer, 1984, **27(10)**, 1879-1891.
[11] Ismaeel, M.E. Heat Transfer in a Square Porous Cavity With Partial Heating and Cooling for Opposite Vertical Walls. Al-Rafadain Engineering Journal, 2011, **19(5)**.
[12] Prasad, V. Convective flow interaction and heat transfer between fluid and porous layers, in Convective Heat and Mass Transfer in Porous Media, 1991, Springer, 563-615.
[13] Kladias, N. and V. Prasad. Flow transitions in buoyancy-induced non-Darcy convection in a porous medium heated from below. Journal of Heat Transfer, 1990, **112(3)**, 675-684.
[14] Kladias, N. and V. Prasad. Natural convection in horizontal porous layers: effects of Darcy and Prandtl numbers. Journal of Heat Transfer, 1989, **111(4)**, 926-935.
[15] Bejan, A. and A.D. Kraus, eds. Heat Transfer Handbook, 2003, John Wiley and Sons.
[16] Hossain, M. and D. Rees. Natural convection flow of a viscous incompressible fluid in a rectangular porous cavity heated from below with cold sidewalls. Heat and Mass Transfer, 2003, **39(8-9)**, 657-663.
[17] Fletcher, C.A.J. Computational techniques for fluid dynamics, 1988, Springer-Verlag: Berlin and New York, p. 493.